

D3HRL: A Distributed Hierarchical Reinforcement Learning Approach Based on Causal Discovery and Spurious Correlation Detection

Chenran Zhao^a, Dianxi Shi^{a,b}, Mengzhu Wang^c, Jianqiang Xia^d, Huanhuan Yang^a, Songchang Jin^b, Shaowu Yang^a, Chunping Qiu^b

^a*College of Computer Science and Technology, National University of Defense Technology, China, Changsha*

^b*Intelligent Game and Decision Lab (IGDL), China, Beijing*

^c*College of Artificial Intelligence, Hebei University of Technology, China, Tianjin*

^d*School of Electronic information and Electrical Engineering, Shanghai Jiao Tong University, China, Shanghai*

Abstract

Current Hierarchical Reinforcement Learning (HRL) algorithms excel in long-horizon sequential decision-making tasks but still face two challenges: delay effects and spurious correlations. To address them, we propose a causal HRL approach called D3HRL. First, D3HRL models delayed effects as causal relationships across different time spans and employs distributed causal discovery to learn these relationships. Second, it employs conditional independence testing to eliminate spurious correlations. Finally, D3HRL constructs and trains hierarchical policies based on the identified true causal relationships. These three steps are iteratively executed, gradually exploring the complete causal chain of the task. Experiments conducted in 2D-MineCraft and MiniGrid show that D3HRL demonstrates superior sensitivity to delay effects and accurately identifies causal relationships, leading to reliable decision-making in complex environments.

Keywords: Causality, Hierarchical Reinforcement Learning, Long-horizon Sequential Decision-making Tasks

1. Introduction

Long-horizon sequential decision-making tasks, which we will refer to as long-horizon tasks, involve achieving a series of intermediate objectives in sequence

to accomplish the ultimate goal. HRL algorithms excel in these tasks due to their inherent framework advantages, yet still face two challenges.

The first challenge is the "delay effect," where temporally extended actions trigger state transitions over multiple time steps, referred to as variable-length state transitions. Submitting papers to a conference exemplifies a temporally extended action with a delay effect, where authors must wait for several months before receiving notification. SMDPs are typically used to model variable-length state transitions. [1] introduced options to simplify SMDPs, proving that SMDPs can be represented as MDPs augmented with options. This abstraction allows agents to make decisions at a more macroscopic level. [2] proposed goals as another form of abstraction, which are typically intermediate states needed to complete the final task. However, both options and goals primarily focus on abstract skills, such as "press the button" [3] or "explore the first room of the maze" [4]. These are combinations of multiple primitive actions rather than the temporal extension of a single action. We aim to incorporate "temporally extended primitive actions" to enable decision-making in more complex tasks.

The second challenge is the spurious correlations. In long-horizon tasks, the complex interactions can lead to widespread data correlations, many of which are spurious. In fact, most agents rely on data correlations rather than causal relationships. [5] show that even powerful ChatGPT is nothing more than an echoing parrot, lacking causal understanding. While these correlation-seeking agents perform well, there is a significant gap between being "usable" and "reliably usable" [6]. For example, a fire breaks out in a residential building, leading to the dispatch of fire trucks and casualties. From a causal perspective, assuming the data is comprehensive and evenly distributed, there are causal relationships as follows: *the dispatch of fire trucks* \leftarrow *fire* \rightarrow *casualties*. This creates an open path between the dispatch of fire trucks and casualties, leading to a correlation between them. In fact, this correlation is spurious and not causal [7]. If an agent learns from these correlations, it might incorrectly infer that dispatching fire trucks will result in casualties, leading to the wrong decision to avoid dispatching them.

To address these challenges, we propose **D3HRL**, a **D**istributed **H**RL approach based on causal **D**iscovery and spurious correlation **D**etection. It iteratively execute the following three modules, progressively uncovering causal chain until the task is completed. **(1) Modeling Delay Effects:** We model delay effects as causal relationships and introduce a distributed causal discovery mechanism to perform parallel learning of causal relationships across various time spans. **(2) Detecting Spurious Correlations:** We conduct conditional independence testing to screen for genuine causal relationships and determine their true time span. **(3) Building**

Hierarchical Policies: We construct hierarchical policy networks and train sub-goals based on the identified causal relationships.

We tested our method in two environments with long-horizon tasks: 2D-MineCraft [8] and MiniGrid [9]. We modified them to enable variable-length state transitions. Results show that D3HRL can identify variable-length state transitions and construct the causal chains accurately, significantly improving the learning efficiency of the hierarchical framework.

2. Related works

2.1. Hierarchical Reinforcement Learning

HRL falls into two categories: option-based (O-HRL) and goal-based (G-HRL). [1] introduced options to model variable-length state transitions in SMDPs, enabling agents to focus on high-level decisions. [2] later introduced goals, breaking tasks into sub-goals to progressively reach the final goal. O-HRL involves a lower-level network learning skills and an upper-level network using these skills, either asynchronously [10, 4, 11] or synchronously [12, 13, 14]. G-HRL involves an upper-level network generating sub-goals and a lower-level network achieving them, typically done synchronously [15, 16, 17, 18]. However, these methods primarily focus on abstract skills rather than temporally extended actions. We propose a distributed causal discovery module and a hierarchical architecture to effectively model them both.

2.2. Causal Reinforcement Learning

Causality integrates with RL in three main ways. First, counterfactual reasoning is used: [19] use counterfactual differential advantage functions to evaluate actions retrospectively, [20] employ counterfactual inference for decisions, and [21] extend Structural Causal Mechanism (SCM) to explain counterfactual behaviors. Second, intrinsic rewards are used: [22] generate rewards by analyzing the causal effect of intermediate variables, guiding policy learning. Third, causal graphs are employed: [23] transform RL into a likelihood maximization problem, learning causal graphs through classification and using them as latent variables for variational inference. However, none of them consider spurious correlations. D3HRL includes a spurious correlation detection module to ensure reliable causal relationships.

2.3. Causal Hierarchical Reinforcement Learning

CHRL is an emerging area. CEHRL [24] uses meta-supervised learning with counterfactual reasoning and advantage functions to learn the hierarchical structure

of control effects. CDHRL [25] gradually learns causal chain through intervention data and build hierarchical policies based on it. Both CEHRL and CDHRL can learn causal chains in long-horizon tasks but fail to model "delayed effects". SCALE [26] uses simulated data to identify causal features and build a skill library, but its reliance on controlled simulations limits autonomous exploration in uncontrolled tasks. COInS [27] identifies key interaction states and constructs skill chains, controlling increasingly difficult factors. However, its skill exploration is manually predefined, not automatic. HCPI-HRL [28] leverages human-guided causal discovery to automatically infer effective and diverse subgoal structures from dynamic environments. The method's dependence on human causal insights curtails its capacity for fully autonomous learning of subgoals and causal structures. VACERL [29] eliminates hand-crafted causal variables by using transformer attention to isolate the observation-action steps most predictive of future returns, then builds a causal graph over those key steps. That graph is converted into intrinsic rewards or sub-goals, sharply boosting exploration in sparse-reward and Noisy-TV tasks. Different from them, our D3HRL employs the automatic gradual exploration of causal chains to complex environments with "delayed effects".

3. Preliminary

Causality [30] refers to a relationship where an intervention on one variable (cause C) directly leads to a change in another variable (effect E), denoted as $C \rightarrow E$. Time series causal discovery involves inferring and quantifying causality from time series data [31], helping to understand the influence mechanisms between variables. Structural causal mechanism (Section 3.1) is used to represent causal relationships. Time series graphical models (Section 3.2) model causal relationships among multiple variables across multiple time steps, and conditional independence testing (Section 3.3) is used to detect spurious correlations.

3.1. Structural Causal Mechanism

Structural Causal Mechanism (SCM). SCM [32] consists of two parts. First is the causal graph, where $C \rightarrow E$ indicates a causal relationship. Second is the generating function, which predicts E based on C .

Granger causality. According to Granger causality [33], if there is a Granger causal relationship between cause C and effect E ($C \rightarrow E$), then C contains unique information related to E that is not contained in all past information (excluding C). The Granger causality test can determine whether a Granger causal relationship

exists between two variables. Leveraging Granger-causality principles, we sample candidate causes C and forecast the effect E ; gains in predictive accuracy reveal the true causal edges. This procedure simultaneously reconstructs the causal graph and learns the generative mapping $E = f(C)$, yielding an instantiation of the SCM.

Intervention. In causal inference, deliberately setting a variable to a specific value and observing the resulting changes is called an *intervention*, denoted by Pearl’s do-operator $\text{do}(C=c)$. In our method, the random sampling of different candidate causes and evaluation of their impact on the prediction of E is tantamount to performing a collection of interventions $\{\text{do}(C=c_i)\}$.

3.2. Time Series Graphical Models

Time Series Graphical Models (TSGM) [34] can model causal relationships across multiple time steps. Figure 1 shows a schematic diagram of a TSGM. Consider a multivariate process X consisting of N variables. Its TSGM can be defined as $G = (\mathbf{V} \times \mathbf{T}, \mathbf{E})$:

- Vertex set $\mathbf{V} = \{\mathbf{X}_t\}_{t=1}^T$: a set of temporal nodes for N variables at each time step $t \in \mathbf{T}$, where $\mathbf{X}_t = \{X_t^1, X_t^2, \dots, X_t^N\}$.
- Edge set \mathbf{E} : a set of causal relationships between nodes in \mathbf{V} . If $X_{t-\tau}^j$ causally influences X_t^i , there is a directed edge $X_{t-\tau}^j \rightarrow X_t^i$ ($\tau > 0$).

The parent nodes of X_t^i , denoted as $\mathcal{PA}(X_t^i)$, are the set of nodes involved in causal relationships where X_t^i is the effect:

$$\mathcal{PA}(X_t^i) = \left\{ X_{t-\tau}^k \mid \begin{array}{l} X_{t-\tau}^k \rightarrow X_t^i \in \mathbf{E}, \tau > 0, \\ X_{t-\tau}^k \in \mathbf{V}, X_t^i \in \mathbf{V} \end{array} \right\} \quad (1)$$

τ_{max} is the maximum time span with significant correlations in complex systems [7]. In other words, τ_{max} is an empirical value that incorporates prior knowledge.

3.3. Conditional Independence Testing

Due to the environmental complexity, determining the information flow along the path $X^j \rightarrow X^i$ is challenging, making it difficult to identify their causal relationship. However, causal theory [30] states that X ’s parent nodes $\mathcal{PA}(X)$ form a sufficient conditioning set to block the backdoor paths, ensuring a unique open path. By evaluating the information flow along this path, we can determine if the variables are conditionally dependent. If they are, it indicates a causal

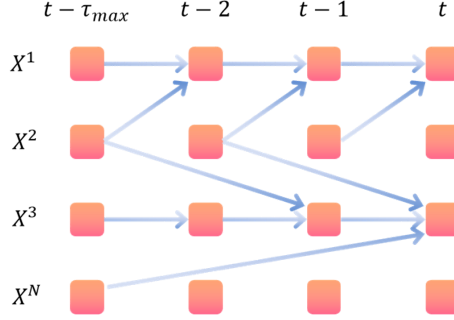


Figure 1: An example of Time Series Graphical Models.

relationship; otherwise, it suggests a spurious correlation. This is known as Conditional Independence Testing (CIT) [7]:

$$X_{t-\tau}^j \perp\!\!\!\perp X_t^i \mid \frac{\mathcal{PA}(X_t^i) \setminus \{X_{t-\tau}^j\}}{\mathcal{PA}(X_{t-\tau}^j)} \Rightarrow X_{t-\tau}^j \nrightarrow X_t^i \quad (2)$$

4. Formalization

Real-world variable-length state transitions can overlap in time but remain independent of each other. For example, after submitting a paper to a conference, one might wait for the notification while working on another project. This paper’s result and the project’s progress are separate sub-states that do not influence each other. We integrate the concepts of SMDPs to model variable-length state transitions and those of Factored-MDPs [35] to handle overlapping sub-state transitions. Besides, state transitions follow objective causal laws. Thus, it is natural to represent variable-length state transitions as causal relationships spanning multiple time steps. Based on these ideas, we propose **Causal Factored-SMDPs**. It relies on several key assumptions:

(1) *Independent Sub-State Transition*: The state can be decomposed into disjoint sub-states [36], and the transitions of each sub-state are independent.

(2) *Cause precedes Effect* [30]: For all $i \neq j$, it holds that $X_t^j \nrightarrow X_t^i$ and $X_t^j \nrightarrow X_{t-\tau}^i$ ($1 \leq \tau \leq \tau_{max}$).

(3) *Causal Sufficiency Assumption* [37]: All relevant causal factors are observed. In our setting, an effect corresponds to multiple causes, and the effect occurs only if all causes meet the conditions, spanning the same time span.

(4) *Causal Markov Condition* [37]: The true causes are sufficient to predict the effect, while other past variables are irrelevant. In our setting, all variables except

actions exhibit autocorrelation.

We replace the state and action spaces with cause and effect spaces, and replace the state transition functions with the generating functions of SCM. We introduce causal relationship matrices and the time span matrix to describe TSGM. Now we present Causal Factored-SMDPs consisting of 5 components $\langle \mathbf{C}, \mathbf{E}, \mathbf{P}, \mathbf{T}, \mathbf{F} \rangle$:

- **Cause Space \mathbf{C} :** Comprises a decomposed state space $\{S^i\}_{i=1}^M \in \mathbf{S} = \{S^1 \times S^2 \times \dots \times S^M\}$ and a decomposed action space $\{A^j\}_{j=1}^N \in \mathbf{A} = \{A^1 \times A^2 \times \dots \times A^N\}$.
- **Effect Space \mathbf{E} :** Comprises a decomposed state space $\{S^i\}_{i=1}^M \in \mathbf{S} = \{S^1 \times S^2 \times \dots \times S^M\}$. The agent's decision is made to induce state transitions, so the action space cannot be considered part of the effect space.
- **Causal Relationship Matrices $\mathbf{P} = \{P_h\}_{h=1}^{\tau_{max}}$:** $P_h \in \{0, 1\}^{(M) \times (M+N)}$ describes the existence of the causal relationships under time span h . $P_h[i][j] = 1$ indicates that C_{t-h}^j is a direct cause of E_t^i , and 0 otherwise.
- **Causal Relationship Time Span Matrix $\mathbf{T} \in \{1, 2, \dots, \tau_{max}\}^{(M) \times (M+N)}$:** The true time span of the causal relationship ($C^j \rightarrow E^i$) is T_{ij} .
- **Causal Effect Generating Functions $\mathbf{F} = \{F_h\}_{h=1}^{\tau_{max}}$:** It consists of generating functions for each time span h and each effect variable E^i :

$$F_h = \left\{ f_h^i(E^i | \mathcal{PA}(E^i)) \mid \begin{array}{l} \mathcal{PA}(E^i) \subseteq \mathbf{C} \\ E^i \in \mathbf{E} \end{array} \right\}_{i=1}^M \quad (3)$$

$f_h^i(E^i | \mathcal{PA}(E^i))$ predicts E^i 's value h steps later given its direct cause $\mathcal{PA}(E^i)$. During these h steps, the value of E^i doesn't change. In short, \mathbf{F} describe the sub-state transitions of each effect variable. Thus, the complete state $S_t = \{E_t^1, E_t^2, \dots, E_t^M\}$ is determined by \mathbf{F} .

5. Approach

In this chapter, we introduce D3HRL, a distributed approach that accurately captures variable-length state transitions and constructs a high-quality hierarchical framework. The overall framework is shown in Figure 2. In Module A, data is collected using a reverse data collection strategy, followed by distributed SCM training to preliminarily identify causal relationships at different time spans (Section 5.1). In Module B, the identified "causal relationships" undergo spurious correlation

detection, including conditional independence testing and determination of causal relationship time spans (Section 5.2). In Module C, based on the identified causal relationships and their time spans, we construct the hierarchical network and train the subgoals for effect variables (Section 5.3). These three modules iteratively execute until the causal chain is explored completely.

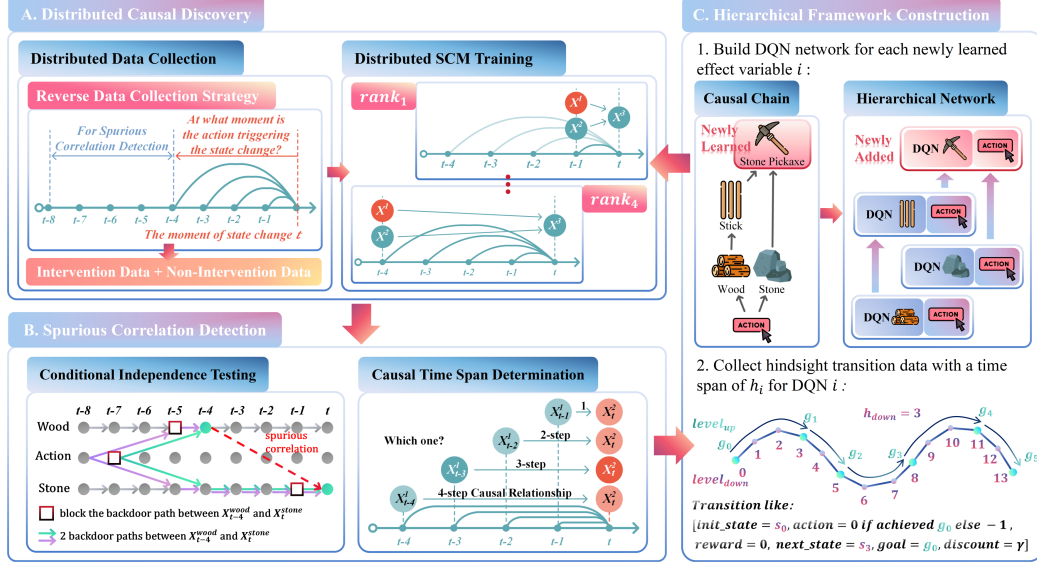


Figure 2: Overview of D3HRL framework.

5.1. Distributed Causal Discovery

To capture the variable-length state transitions, we propose a distributed causal discovery method consisting of distributed data collection and distributed SCM training. Based on the maximum time span τ_{max} , multiple processes $\{rank_h\}_{h=1}^{\tau_{max}}$ are set up for distributed learning.

5.1.1. Distributed Data Collection.

Each process $rank_h$ interacts with the environment using the current hierarchical policy in an offline manner. Complete trajectories are stored in the replay buffer \mathbf{R} and extracted for data collection. We employ a reverse data collection strategy: after an intervention variable $X_{do} \in List_{do}$ (initially $List_{do} = \{\mathbf{A}\}$) is triggered, if the state changes at t , given τ_{max} , the causes must lie within $[t - \tau_{max}, t)$. Therefore, starting from t , we collect $\tau_{max} + 1$ steps of data in reverse:

$$d_t^{scm} = \{s_{t-\tau_{max}}, a_{t-\tau_{max}}, \dots, s_{t-1}, a_{t-1}, s_t, a_t\} \quad (4)$$

Additionally, to facilitate the detection of spurious correlations, we also collect an additional τ_{max} steps of data in reverse:

$$d_t^{cmi} = \{s_{t-2\tau_{max}}, a_{t-2\tau_{max}}, \dots, a_{t-\tau_{max}-1}\} \quad (5)$$

For each iteration, we collect $batch_size$ such segments of intervention data for each intervention variable parallelly:

$$D_{do} = \left\{ D_{do}^h = \left\{ cat(d_{t_k}^{cmi}, d_{t_k}^{scm}) \right\}_{k=1}^{batch_size/\tau_{max}} \right\}_{h=1}^{\tau_{max}} \quad (6)$$

Furthermore, to contrast with cases where X_{do} is not triggered, we collect an equal amount of non-intervention data D_{undo} . This is done by sliding and collecting data segments from the start of each episode until the required amount is reached, as long as X_{do} is not triggered. The parallelly collected data $\mathbf{D} = \{D_{do}, D_{undo}\}$ is then redistributed to all processes. Reverse strategy more effectively traces the multiple causes of state changes compared to the forward strategy.

5.1.2. Distributed SCM Training.

Each process $rank_h$ trains SCM under the time span h based on the collected data \mathbf{D} . As shown in Figure 2.A, given $\tau_{max} = 4$, process $rank_1$ handles 1-step causal relationships $X_{t-1}^j \rightarrow X_t^i$ and process $rank_4$ handles 4-step causal relationships $X_{t-4}^j \rightarrow X_t^i$. We adapted the SCM training methods from CDHRL and SDI [38]. For SCM_h with $M+N$ variables $\{X_k\}_{k=1}^{M+N}$, we construct two parts of networks: generating functions $F_h = \{f_h^i(\theta)\}_{i=1}^M$ and a causal graph's parameter matrix $\eta_h \in \mathbb{R}^{M \times (M+N)}$. Generating functions: $f_h^i(\theta)$ predicts the value of X^i given its direct cause set. During training, based on the sampled causal relationship matrix P_h and collected data \mathbf{D} , we input the causes $\mathcal{PA}(X_t^i) = \{X_{t-h}^j | P_h[i][j] = 1\}$ of each effect X_t^i into $f_h^i(\theta)$ to evaluate the likelihood \mathcal{L} . The true value X_t^i serves as the label to maximize \mathcal{L} , thereby updating $f_h^i(\theta)$:

$$\max \mathcal{L}(\theta | X_t^i) = \log_softmax(f_h^i(X_t^i | \mathcal{PA}(X_t^i); \theta)) \quad (7)$$

Causal graph's parameter matrix: $\sigma(\eta_h^{ij}) = 1/(1 + e^{-\eta_h^{ij}})$ represents the probability that X^j is a direct cause of X^i with a time span h . During training, we sample K batches of data $\{D^k\}_{k=1}^K$ from \mathbf{D} and N_p causal relationship matrices $\{P_h^n\}_{n=1}^{N_p}$, calculate the likelihood $\mathcal{L}(P_h^n, D^k)$ for each effect X^i and compute the gradient ∇_{η_h} as follows:

$$\nabla_{\eta_h} = \sum_k \left[\sum_n (\sigma(\eta) - P_h^n) \right] \left(\frac{e^{\sum_n \mathcal{L}(P_h^n, D^k)}}{\sum_{k'} e^{\sum_n \mathcal{L}(P_h^n, D^{k'})}} \right) \quad (8)$$

In each iteration, matrix η_h is trained after functions F_h have converged. Then we use $\sigma(\eta_h)$ to preliminarily identify causal relationships where causes are in $List_{do}$ and effects are not, ensuring the learned causal graph remains a DAG. Typically, if $\sigma(\eta_h^{ij}) \geq 0.8$, then $X^j \xrightarrow{h} X^i$ exists [25].

5.2. Spurious Correlation Detection

Common causes can create non-zero information flow between variables that originally have no causal relationship, leading to spurious correlations. Besides, autocorrelation may result in the identification of causal relationships with incorrect time spans, another form of spurious correlation. Therefore, after training SCM_h , it is essential to filter out spurious correlations to ensure the validity of the learned causal graph.

5.2.1. Conditional Independence Testing.

As shown in Figure 2.B, the causality $stone \xleftarrow{3} \mathbf{A} \xrightarrow{3} wood$ and $wood$'s auto-correlation create an information flow between X_{t-4}^{wood} and X_t^{stone} , leading the SCM to misidentify a spurious correlation as a causal link. As discussed in Section 3.3, conditioning on the parents (denoted by \square) blocks backdoor paths, ensuring $X_{t-4}^{wood} \rightarrow X_t^{stone}$ is the only open path between them. Then we can use CIT to determine whether this correlation is spurious. In fact, CIT can be transformed into the evaluation of whether the corresponding Conditional Mutual Information (CMI) is greater than zero [39, 40]: $X \perp\!\!\!\perp Y \mid Z \Leftrightarrow I(X; Y \mid Z) = 0$. Thus we use CMI to perform CIT for any given correlation $X_{t-h}^j \rightarrow X_t^i$:

$$\begin{aligned}
& I(X_{t-h}^j; X_t^i | \mathcal{PA}(X_t^i) \setminus X_{t-h}^j, \mathcal{PA}(X_{t-h}^j)) \\
&= H[X_t^i | \mathcal{PA}(X_t^i) \setminus X_{t-h}^j, \mathcal{PA}(X_{t-h}^j)] \\
&\quad - H[X_t^i | \mathcal{PA}(X_t^i), \mathcal{PA}(X_{t-h}^j)] \\
&= E \left[-\log p(X_t^i | \mathcal{PA}(X_t^i) \setminus X_{t-h}^j, \mathcal{PA}(X_{t-h}^j)) \right. \\
&\quad \left. + \log p(X_t^i | \mathcal{PA}(X_t^i), \mathcal{PA}(X_{t-h}^j)) \right]
\end{aligned} \tag{9}$$

For each effect variable X^i , we construct a 3-layer fully connected neural network $g(\phi_i)$ to compute the likelihood conditioned on the parents: $\hat{p}_{\phi_i}(X_t^i | \mathcal{PA}(X_t^i) \setminus X_{t-h}^j, \mathcal{PA}(X_{t-h}^j))$ and $\hat{p}_{\phi_i}(X_t^i | \mathcal{PA}(X_t^i), \mathcal{PA}(X_{t-h}^j))$. During training, we randomly sample sequences of $2\tau_{max} + 1$ consecutive data points from replay buffer

R. Input the values of $\mathcal{PA}(X_t^i)$ and $\mathcal{PA}(X_{t-h}^j)$ into $g(\phi_i)$, mask either $\{None, X_{t-h}^j\}$ randomly and update ϕ_i by maximizing the likelihood until convergence. After training, we use the collected data \mathbf{D} to evaluate the expected CMI of the correlation according to Equation 9:

$$\begin{aligned} \hat{I}_{\phi_i}(X_{t-h}^j \rightarrow X_t^i) \\ = E \left[-\log \hat{p}_{\phi_i}(X_t^i | \mathcal{PA}(X_t^i) \setminus X_{t-h}^j, \mathcal{PA}(X_{t-h}^j)) \right. \\ \left. + \log \hat{p}_{\phi_i}(X_t^i | \mathcal{PA}(X_t^i), \mathcal{PA}(X_{t-h}^j)) \right] \end{aligned} \quad (10)$$

In practice, due to data errors, we consider correlations with CMI above threshold ϵ_{cmi} as genuine causal relationships:

$$\hat{I}_{\phi_i}(X_{t-h}^j \rightarrow X_t^i) > \epsilon_{cmi} \Rightarrow X_{t-h}^j \rightarrow X_t^i \quad (11)$$

5.2.2. True Causal Relationships and Time Span Determination.

A causal relationship between two variables might be judged to be valid across multiple different time spans. TSGM reveals that, apart from the true time span h_i , other cases may arise from the combination of a direct causal relationship ($X_{t-h}^j \xrightarrow{h_i} X_t^i$) and a variable's autocorrelation ($X_t^i \rightarrow X_{t+1}^i$), leading to indirect causation ($X_{t-h}^j \xrightarrow{h_i+1} X_{t+1}^i$). Typically, causal paths with collider structures lead to independence, making it unlikely for a causal relationship to appear with a time span shorter than the true time span. Therefore, if $X^j \rightarrow X^i$ is judged to be valid across multiple different time spans, the shortest one is identified as true.

Throughout training, any correlation identified by SCM is tested for spuriousness. Once confirmed as a causal relationship and successfully trained as a subgoal, it is not retested. Furthermore, it is important to note that early intervention data may not be sufficient to uncover deeper causality. Spurious correlations identified in earlier iterations might become genuine later. Thus, each iteration's identification of spurious correlations serves as a reference only for that iteration.

5.3. Hierarchical Policy Training

D3HRL adopts the progressive causal chain learning idea from CDHRL [25], constructing and training hierarchical policies based on the learned causal chain.

5.3.1. The Construction of the Hierarchical Policy Network.

We implement D3HRL based on multi-level DQN [41] with HER [42]¹. In each iteration, after determining the true causality, a sub-goal network is established for each newly-learned effect variable with its action space set to include the causes of the effect and the primitive action space \mathbf{A} . For example, as shown in Figure 2.C, we add a new DQN sub-goal network for the newly-learned effect variable *stonepickaxe* (denoted as X^{sp}), given the newly-learned causality ($stone \xrightarrow{h_{sp}} stonepickaxe \xleftarrow{h_{sp}} stick$). Its action space is set to $A_{sp} = \{g_{stone}, g_{stick}, \mathbf{A}\}$. In addition, there is always a top-level network with action space $A_{top} = \{trained\ sub\text{-}goals, currently\ training\ sub\text{-}goals, \mathbf{A}\}$. When the causal chain in the environment is fully explored, the resulting hierarchical policy network closely mirrors the causal chain. At this point, we simply input the target into the top-level network, which can then recursively trace the causes and sequentially achieve them.

5.3.2. The Training of the Hierarchical Policy Network.

During the training of the sub-goal network for X^{sp} , it learns to invoke the sub-goal networks for *stone* ($action=g_{stone}$) and *stick* ($action=g_{stick}$) to increase or decrease their quantities, and to generate *stonepickaxe* (sub-goal g_{sp}) after obtaining the necessary materials ($action \in \mathbf{A}$). To handle variable-length state transitions, we adapt the hindsight transition collection mechanisms of CDHRL and HER. Specifically, at each time step t during interaction with the environment, we log the 1-step transition and extract the continuous $h_{sp} + 1$ steps of data: $\{s_{t-h_{sp}}, a_{t-h_{sp}}, \dots, s_t, a_t\}$. Based on whether g_{sp} is achieved within this period, we generate hindsight goal transition: $[initial\ state=s_{t-h_{sp}}, action=a_{t-h_{sp}}, reward=0\ if\ achieved\ g_{sp}\ else\ -1, next\ state=s_t, goal=g_{sp}, discount=\gamma]$. We then obtain the sub-goals achieved during this period, denoted as G_{ach} . For each sub-goal $g_i \in G_{ach}$, we generate hindsight action transition: $[initial\ state=s_{t-h_{sp}}, action=g_i, reward=0\ if\ achieved\ g_{sp}\ else\ -1, next\ state=s_t, goal=g_{sp}, discount=\gamma]$. Each sub-goal network is trained on the collected hindsight transition data and, after successfully trained, added to $List_{do} = \{\mathbf{A}, X^{sp}\}$ for the next iteration to begin.

¹We implement D3HRL based on the code of CDHRL

6. Experiment

6.1. Experiment Setup

Environment. We introduce two environments: 2D-MineCraft [8] and MiniGrid [9]. Both feature long-horizon sequential decision-making tasks with rewards provided only upon task completion. We designed two tasks for each: GetIron and GetSilverore for 2D-MineCraft, and Fire2Burn and Wood2Wet for MiniGrid. Take the GetIron task as an example, where the agent must obtain iron within a limited time. This involves sequentially gathering wood and stone, crafting sticks, creating a stone axe, collecting iron ore and coal, and finally smelting the iron. All tasks in our setting are sequential decision-making tasks like this. We modified these tasks to support variable-length state transitions. "T0~3" suffixes denote various time span configurations, where "T0" indicates that all state transitions in the environment are single-step ($\tau_{max} = 1$), and "T1", "T2", and "T3" represent three distinct configurations of state transition spans under $\tau_{max} = 4$. "R0~1" suffixes denote resource levels: "R1" for abundant, "R0" for scarce.

Evaluation Metrics. We use Average Success Ratio (**ASR**) and Average Distance to Complete task (**ADC**) over the most recent 100 episodes during training as metrics. Higher ASR indicates better task completion, and lower ADC indicates deeper causal chain exploration. We also use Structural Hamming Distance (**SHD**) to measure the accuracy of the learned causal relationship graphs. Lower SHD indicates a more accurate causal relationship graph. All results are averaged over 5 random seeds.

Baselines. We compare D3HRL with CDHRL [25], HAC [43], Option-Critic [44] and LESSON [45]. **CDHRL** and D3HRL are both CHRL methods that learn goal-based hierarchical policies using sequential causal chain learning. **HAC** is a powerful goal-based HRL method that utilizes three types of transitions to steadily train hierarchical policies. **Option-Critic** is the first framework to use options for modeling variable-length state transitions. **LESSON** is a unified exploration framework based on Option-Critic. **We enhanced the baselines to identify causal relationships and adapt to variable-length state transitions.** For algorithms that cannot identify causal relationships, we designed a curriculum to help them learn sub-goals progressively. For those that cannot perceive variable-length state transitions, we set the transition data collection span to τ_{max} , enabling them to perceive transitions within τ_{max} steps.

6.2. Experimental Results

We design experiments to answer the following questions:

6.2.1. How does D3HRL perform on long-horizon sequential decision-making tasks compared to the baselines?

Experimental Design. We compared D3HRL with the enhanced baselines in terms of ASR and ADC on four tasks with different configurations. The results are shown in Figure 3.

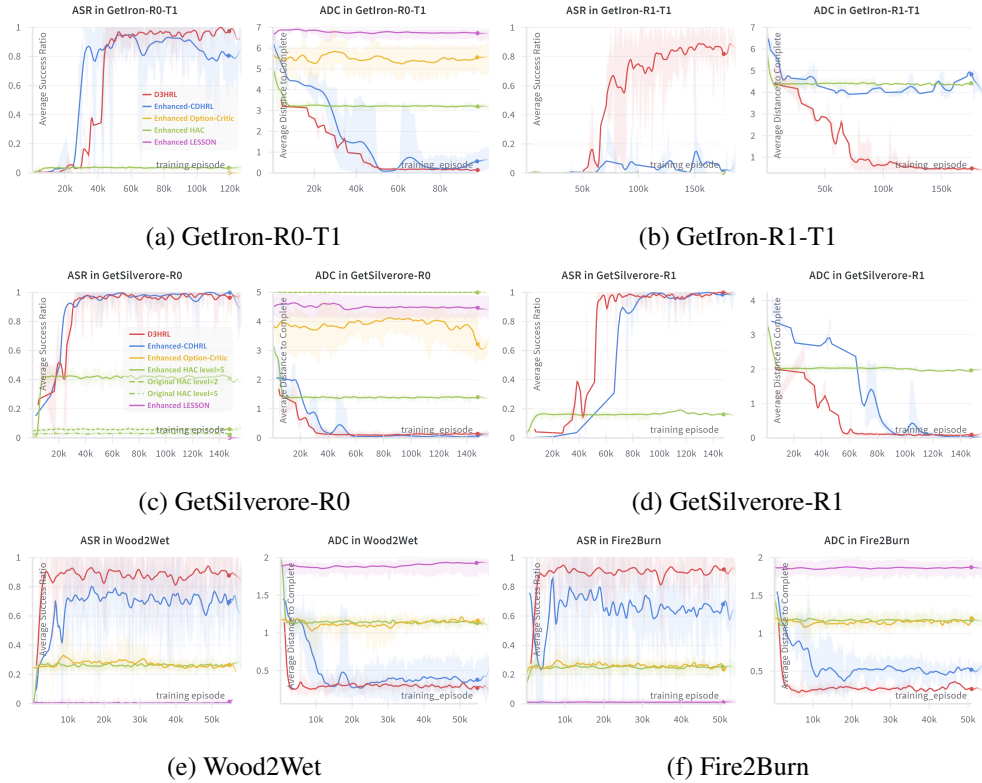


Figure 3: ASR and ADC under MiniGrid and MineCraft tasks.

Experimental Results. **D3HRL** effectively identifies variable-length state transitions and filters out spurious correlations, performing best even in tasks with scarce resources. **CDHRL** initially outperforms D3HRL by learning indirect causality, enabling early exploration of deeper causality. However, its inability to accurately

identify causality leads to greater complexity in sub-goal training, ultimately resulting in suboptimal performance. **HAC** can only explore up to 3.8 layers of the causal chain. Unlike CDHRL and D3HRL, which learn causality autonomously, HAC uses pre-defined curriculum to directly acquire causality, leading to earlier success. However, it struggles with variable-length state transitions. Multiple sub-goals in the same layer, with varying time spans, complicate training and hinder progress on deeper goals. Scarce resources make it hard for HAC and CDHRL to gather materials, resulting in low success. **Option-Critic** performs well in MiniGrid tasks with shallow causal chains but struggles in MineCraft tasks with deeper causal chains. While it can handle variable-length state transitions, its lack of a multi-layer policy structure prevents it from recalling previously learned sub-goals, despite having a curriculum for sequential sub-goal learning. This leads to decreasing efficiency in sub-goal learning and failure to complete the subsequent curriculum, especially in tasks with deep causal chains. **LESSON** consistently fails across all tasks since it lacks a multi-layer policy structure and cannot remember previously learned sub-goals, and it treats each option as an exploration strategy rather than a skill, making it ineffective in training sub-goals.

6.2.2. *Experiment Validation: How does the reverse data collection strategy compare to the forward data collection strategy?*

Experimental Design. We evaluate two strategies on causal relationship learning in GetIron-R0 with $\tau_{max} = 4$. For a fair comparison, each causal relationship was learned assuming the preceding ones were already known. Additionally, the causal probability for each new segment was initialized to 0.5. Results are shown in Figure 4. Each figure contains up to 8 curves, representing the causality existence probability of the causal relationships as indicated in the figure titles at different time spans $h \in \{1, 2, 3, 4\}$, four are solid lines for reverse strategy, four are dashed lines for forward strategy.

Experimental Results. It can be observed that the convergence rate of the causal relationship learning curve is higher with the reverse data collection strategy compared to the forward strategy for most causal relationships, thereby validating the effectiveness of our reverse data collection strategy.

6.2.3. *How does D3HRL compare to CDHRL in terms of the accuracy of causal graph identification?*

Experimental Design. To ensure a fair comparison, we evaluate the SHD of causal graphs identified by CDHRL and D3HRL in GetIron-R0 task and Wood2Wet

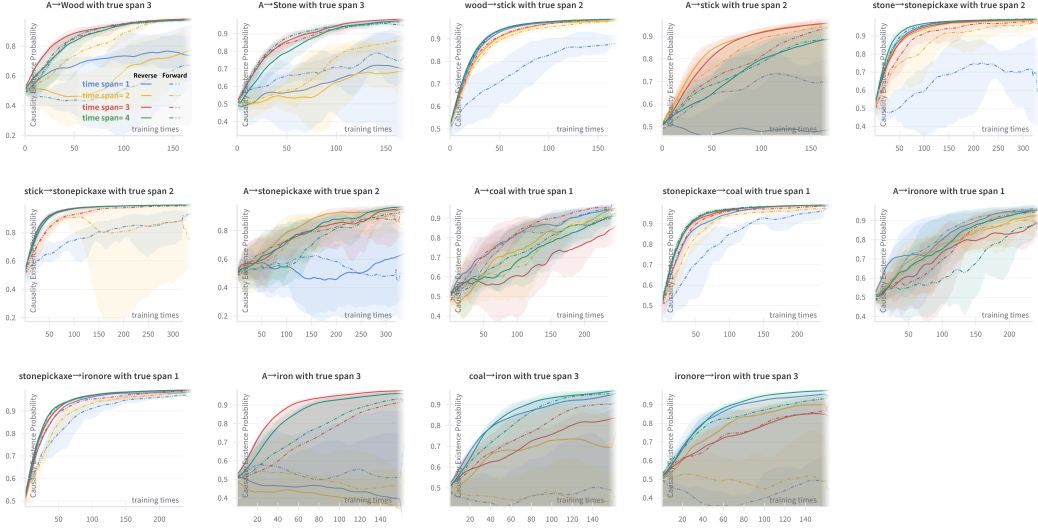


Figure 4: The comparison between reverse and forward data collection strategy in GetIron-R0-T1 task with $\tau_{max} = 4$.

task with $\tau_{max} = 1$ and $\tau_{max} = 4$, the result is shown in Table 1. Figures 5 presents the causal relationship matrices learned by CDHRL in GetIron-R0-T0 ($\tau_{max} = 1$) task and GetIron-R0-T1 ($\tau_{max} = 4$) respectively. Figures 6 presents the causal relationship matrices learned by D3HRL in GetIron-R0-T0 ($\tau_{max} = 1$) task and GetIron-R0-T1 ($\tau_{max} = 4$) respectively. In these causal matrices, the rows represent effect variables X^j , and the columns represent cause variables X^i . If D3HRL identifies a causal relationship $X^i \rightarrow X^j$, the corresponding element in the matrix is 1; otherwise, it is 0. Notably, in the causal relationship matrices learned by D3HRL, the numbers indicate the time spans of the causal relationships.

Method \ Task (τ_{max})	GetIron-R0		Wood2Wet			
	1	4	1	4	8	16
CDHRL	21.4	24	1	1	\	\
D3HRL (ours)	3.4	2	0.2	0.4	0.4	0.2

Table 1: The SHD of CDHRL and D3HRL under various tasks and τ_{max} .

Experimental Results. As shown in Table 1, D3HRL consistently achieves lower SHD across all tasks, indicating that it outperforms CDHRL in terms of causal graph accuracy in both $\tau_{max} = 1$ and $\tau_{max} = 4$ tasks. By comparing these causal relationship matrices learned by CDHRL and D3HRL in Figure 5 and Figure 6, it becomes evident that the causal relationship matrices learned by CDHRL includes numerous spurious correlations. In contrast, D3HRL accurately identifies the causal relationship matrices and the time spans of the corresponding causal relationships.

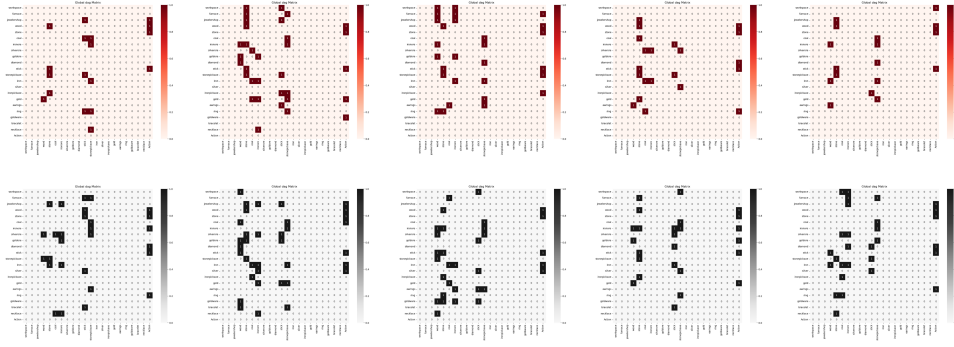


Figure 5: The causal graph matrices of CDHRL in GetIron-R0-T0 task (up) and GetIron-R0-T1 task (down).

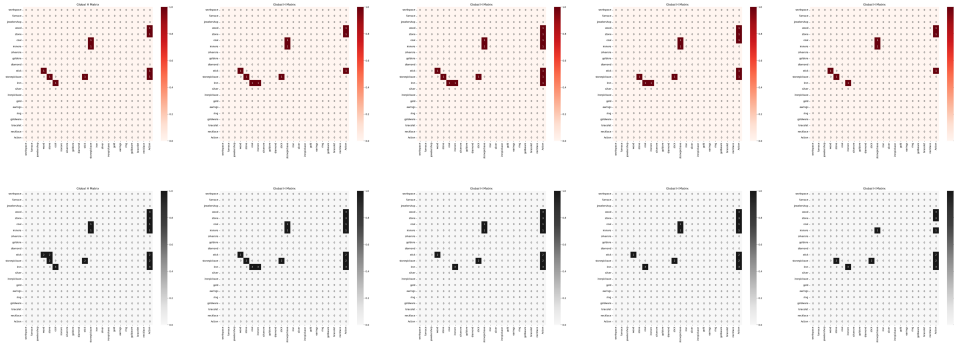


Figure 6: The causal graph matrices of D3HRL in GetIron-R0-T0 task (up) and GetIron-R0-T1 task (down).

6.2.4. How does DEHRL perform in the generalization of identifying causal graphs?

Experimental Design. To validate the generalization of D3HRL in identifying causal graphs, we recorded the causal graphs identified by D3HRL on the GetIron task under various causal time span configurations, the results are shown in Figure 7.

Experimental Results. The results indicate that D3HRL consistently produces accurate causal graphs across different configurations. This clearly demonstrates D3HRL’s robust generalization in causal graph identification.

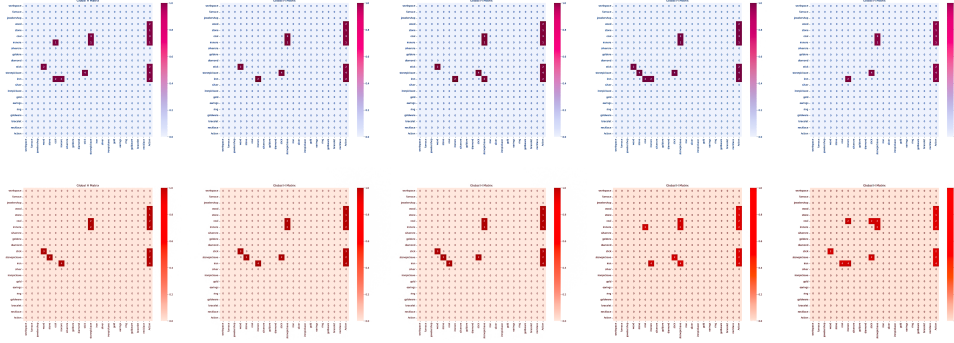


Figure 7: The learned causal graph matrices of D3HRL in GetIron-R0-T2 task (up) and GetIron-R0-T3 task (down).

6.2.5. Does D3HRL filter out spurious correlations?

Experimental Design. We record the CMI values of partial correlations evaluated by the spurious correlation detection module in GetIron-R0-T1, as shown in Figures 8 and 9. Figure 8 shows CMI values for true causal relationships. Figure 9 shows CMI values for spurious correlations, the first 12 figures are for indirect causal relationships, while the last 2 figures are for spurious correlations. The x-axis denotes the iteration, and the y-axis denotes the CMI value. With $\tau_{max} = 4$, each figure contains up to 4 curves, representing the CMI values of the correlations as indicated in the figure titles at various time spans $h \in \{1, 2, 3, 4\}$.

Experimental Results. It is observed that spurious correlations have CMI values of 0, and most indirect causal relationships have CMI values much less than 0.05. In contrast, most direct causal relationships at their true time spans have CMI

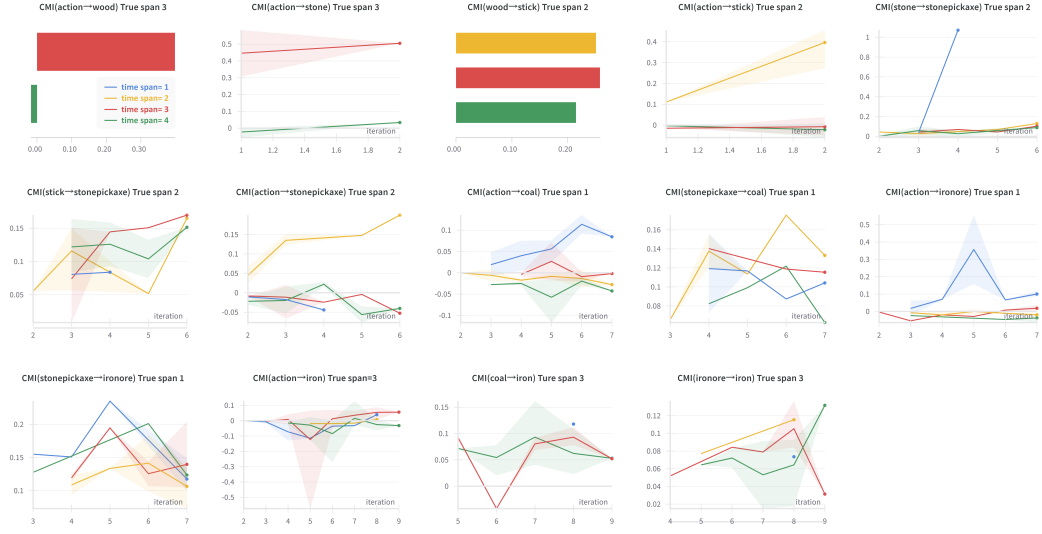


Figure 8: The CMI of different time spans of **causal relationships** in GetIron-R0-T1 task with $\tau_{max} = 4$.

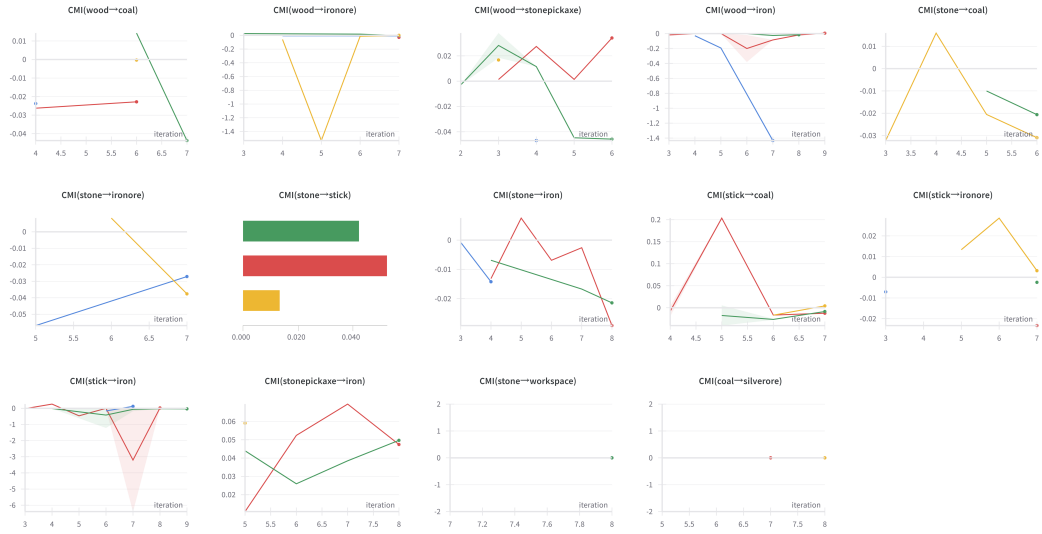


Figure 9: The CMI of different time spans of **spurious correlations** in GetIron-R0-T1 task with $\tau_{max} = 4$.

values significantly greater than 0.05. Therefore, the CIT through CMI effectively distinguishes spurious correlations from causal relationships with $\epsilon_{cmi} = 0.05$. For example, the second subplot in Fig 4 shows the CMI values for the relationship $A \rightarrow stone$ across 4 various time spans. This relationship (with time spans 3 and 4) was preliminarily identified as a true causality by SCM in the 1st and 2nd iterations and underwent spurious correlation detection (SCD). In the 2nd iteration, it passed SCD and was mastered by the hierarchical policy (thus no further SCD was operated), with the CMI value at time span 3 exceeding $\epsilon_{cmi} = 0.05$, but not at 4. Thus, the true time span was determined to be 3, consistent with the truth. For the first and third subplots of Fig 4, these relationships passed SCD and were mastered in one iteration, thus only one iteration of CMI values is shown as bar charts. It is important to note that the selection of ϵ_{cmi} was determined through a separate statistical experiment conducted prior to our main experiments. Statistical analysis revealed that choosing $\epsilon_{cmi} = 0.05$ is suitable for our tasks.

6.2.6. How does D3HRL compare to CDHRL in terms of the quality of the hierarchical framework?

Experimental Design. To ensure a fair comparison, we compared the sub-goals training efficiency of D3HRL and CDHRL in GetIron-R0-T0 ($\tau_{max} = 1$) and GetIron-R0-T1 ($\tau_{max} = 4$) tasks, as shown in Figure 10.

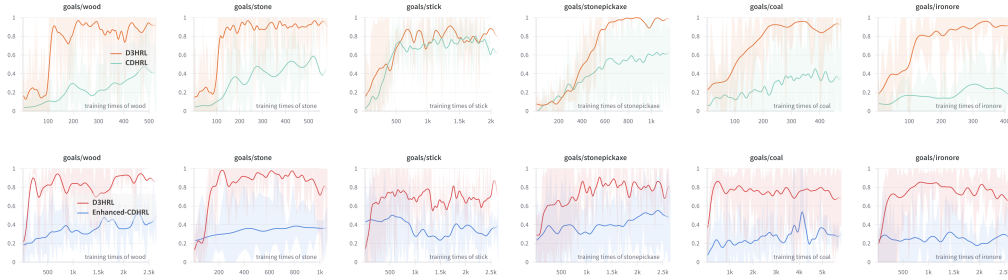


Figure 10: Comparison of sub-goal training efficiency in GetIron-R0-T0 with $\tau_{max} = 1$ (Up) and GetIron-R0-T1 with $\tau_{max} = 4$ (Down).

Experimental Results. The results indicate that D3HRL demonstrates higher training efficiency for most sub-goals compared to CDHRL, achieving better sub-goal completion in shorter training times in both $\tau_{max} = 1$ and $\tau_{max} = 4$ tasks. Overall, the hierarchical framework employed by D3HRL proves to be more efficient in training sub-goals.

6.2.7. Scalability: How does D3HRL perform across different time spans?

Experimental Design. To validate the ASR of D3HRL under different time spans and the SHD of its causal graph identification, we conducted experiments in Wood2Wet task, varying the values of τ_{max} to 1, 4, 8, and 16. The results are shown in Figure 11 and Table 1.

Experimental Results. As depicted in Figure 11 and Table 1, D3HRL accurately captures causal relationships in tasks with long state transition spans and performs consistently well across tasks with varying maximum transition spans. In summary, the final average success rates are similar, indicating that the maximum time span (number of parallel processes) has little impact on the learning of causal relationships. However, increasing the number of parallel processes can lead to longer experimental times, especially with limited hardware resources.

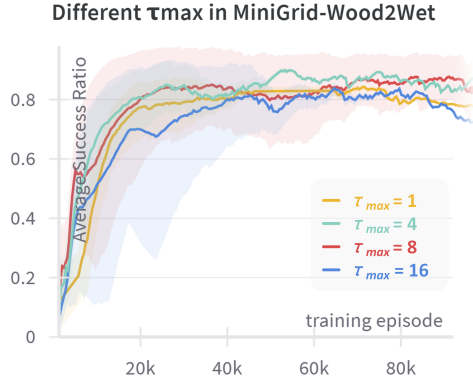


Figure 11: D3HRL’s ASR in MiniGrid-Wood2Wet task with varying τ_{max} .

7. Conclusion

Existing HRL methods face two key challenges in long-horizon tasks: delay effects (variable-length state transitions) and spurious correlations. D3HRL addresses them by modeling variable-length state transitions with distributed causal discovery and filtering out spurious correlations using conditional independence testing. However, D3HRL struggles with tasks that have randomly distributed time spans and is limited to tasks with decouplable state variables. Future work will extend D3HRL to handle diverse modalities, such as images, and manage tasks with randomly distributed state transitions.

References

- [1] R. S. Sutton, D. Precup, S. Singh, Between mdps and semi-mdps: A framework for temporal abstraction in reinforcement learning, *Artificial intelligence* 112 (1-2) (1999) 181–211.
- [2] T. Schaul, D. Horgan, K. Gregor, D. Silver, Universal value function approximators, in: *International conference on machine learning*, PMLR, 2015, pp. 1312–1320.
- [3] F. Röder, M. Eppe, P. D. Nguyen, S. Wermter, Curious hierarchical actor-critic reinforcement learning, in: *Artificial Neural Networks and Machine Learning–ICANN 2020: 29th International Conference on Artificial Neural Networks*, Bratislava, Slovakia, September 15–18, 2020, *Proceedings, Part II* 29, Springer, 2020, pp. 408–419.
- [4] V. Campos, A. Trott, C. Xiong, R. Socher, X. Giró-i Nieto, J. Torres, Explore, discover and learn: Unsupervised discovery of state-covering skills, in: *International Conference on Machine Learning*, PMLR, 2020, pp. 1317–1327.
- [5] M. Willig, M. Zecevic, D. S. Dhimi, K. Kersting, Causal parrots: Large language models may talk causality but are not causal, preprint 8 (2023).
- [6] Z. Deng, J. Jiang, G. Long, C. Zhang, Causal reinforcement learning: A survey, arXiv preprint arXiv:2307.01452 (2023).
- [7] J. Runge, P. Nowack, M. Kretschmer, S. Flaxman, D. Sejdinovic, Detecting and quantifying causal associations in large nonlinear time series datasets, *Science advances* 5 (11) (2019) eaau4996.
- [8] S. Sohn, J. Oh, H. Lee, Hierarchical reinforcement learning for zero-shot generalization with subtask dependencies, *Advances in neural information processing systems* 31 (2018).
- [9] M. Chevalier-Boisvert, B. Dai, M. Towers, R. de Lazcano, L. Willems, S. Lahlou, S. Pal, P. S. Castro, J. Terry, Minigrid & miniworld: Modular & customizable reinforcement learning environments for goal-oriented tasks, CoRR abs/2306.13831 (2023).
- [10] B. Eysenbach, A. Gupta, J. Ibarz, S. Levine, Diversity is all you need: Learning skills without a reward function, arXiv preprint arXiv:1802.06070 (2018).

- [11] J. Achiam, H. Edwards, D. Amodei, P. Abbeel, Variational option discovery algorithms, arXiv preprint arXiv:1807.10299 (2018).
- [12] K. Frans, J. Ho, X. Chen, P. Abbeel, J. Schulman, Meta learning shared hierarchies, arXiv preprint arXiv:1710.09767 (2017).
- [13] Y. Song, J. Wang, T. Lukasiewicz, Z. Xu, M. Xu, Diversity-driven extensible hierarchical reinforcement learning, in: Proceedings of the AAAI conference on artificial intelligence, Vol. 33, 2019, pp. 4992–4999.
- [14] S. Song, J. Weng, H. Su, D. Yan, H. Zou, J. Zhu, Playing fps games with environment-aware hierarchical reinforcement learning., in: IJCAI, 2019, pp. 3475–3482.
- [15] S. Park, D. Ghosh, B. Eysenbach, S. Levine, Hiql: Offline goal-conditioned rl with latent states as actions, Advances in Neural Information Processing Systems 36 (2024).
- [16] Q. Zou, E. Suzuki, Sample-efficient goal-conditioned reinforcement learning via predictive information bottleneck for goal representation learning, in: 2023 IEEE International Conference on Robotics and Automation (ICRA), IEEE, 2023, pp. 9523–9529.
- [17] Y. Li, Y. Wang, X. Tan, Highly valued subgoal generation for efficient goal-conditioned reinforcement learning, Neural Networks 181 (2025) 106825.
- [18] W. Ou, B. Luo, B. Wang, Y. Zhao, Modular hierarchical reinforcement learning for multi-destination navigation in hybrid crowds, Neural Networks 171 (2024) 474–484.
- [19] J. Foerster, G. Farquhar, T. Afouras, N. Nardelli, S. Whiteson, Counterfactual multi-agent policy gradients, in: Proceedings of the AAAI conference on artificial intelligence, Vol. 32, 2018.
- [20] L. Buesing, T. Weber, Y. Zwols, S. Racaniere, A. Guez, J.-B. Lespiau, N. Heess, Woulda, coulda, shoulda: Counterfactually-guided policy search, arXiv preprint arXiv:1811.06272 (2018).
- [21] P. Madumal, T. Miller, L. Sonenberg, F. Vetere, Explainable reinforcement learning through a causal lens, in: Proceedings of the AAAI conference on artificial intelligence, Vol. 34, 2020, pp. 2493–2500.

- [22] T. Herlau, R. Larsen, Reinforcement learning of causal variables using mediation analysis, in: *Proceedings of the AAAI Conference on Artificial Intelligence*, Vol. 36, 2022, pp. 6910–6917.
- [23] W. Ding, H. Lin, B. Li, D. Zhao, Generalizing goal-conditioned reinforcement learning with variational causal reasoning, *Advances in Neural Information Processing Systems* 35 (2022) 26532–26548.
- [24] O. Corcoll, R. Vicente, Disentangling controlled effects for hierarchical reinforcement learning, in: *Conference on Causal Learning and Reasoning*, PMLR, 2022, pp. 178–200.
- [25] X. Hu, R. Zhang, K. Tang, J. Guo, Q. Yi, R. Chen, Z. Du, L. Li, Q. Guo, Y. Chen, et al., Causality-driven hierarchical structure discovery for reinforcement learning, *Advances in Neural Information Processing Systems* 35 (2022) 20064–20076.
- [26] T. E. Lee, S. Vats, S. Girdhar, O. Kroemer, Scale: Causal learning and discovery of robot manipulation skills using simulation, in: *CoRL 2023 Workshop on Learning Effective Abstractions for Planning (LEAP)*, 2023.
- [27] C. Chuck, K. Black, A. Arjun, Y. Zhu, S. Niekum, Granger causal interaction skill chains, *Transactions on Machine Learning Research*.
- [28] B. Chen, Z. Cao, W. Mayer, M. Stumptner, R. Kowalczyk, Hcpi-hrl: Human causal perception and inference-driven hierarchical reinforcement learning, *Neural Networks* 187 (2025) 107318.
- [29] M. H. Nguyen, H. Le, S. Venkatesh, Variable-agnostic causal exploration for reinforcement learning, in: *Joint European Conference on Machine Learning and Knowledge Discovery in Databases*, Springer, 2024, pp. 216–232.
- [30] J. Pearl, *Models, reasoning and inference*, Cambridge, UK: Cambridge University Press 19 (2) (2000) 3.
- [31] J. Runge, S. Bathiany, E. Bollt, G. Camps-Valls, D. Coumou, E. Deyle, C. Glymour, M. Kretschmer, M. D. Mahecha, J. Muñoz-Marí, et al., Inferring causation from time series in earth system sciences, *Nature communications* 10 (1) (2019) 2553.

- [32] J. Peters, D. Janzing, B. Schölkopf, Elements of causal inference: foundations and learning algorithms, The MIT Press, 2017.
- [33] C. W. Granger, Investigating causal relations by econometric models and cross-spectral methods, *Econometrica: journal of the Econometric Society* (1969) 424–438.
- [34] M. Eichler, Graphical modelling of multivariate time series, *Probability Theory and Related Fields* 153 (2012) 233–268.
- [35] C. Boutilier, T. Dean, S. Hanks, Decision-theoretic planning: Structural assumptions and computational leverage, *Journal of Artificial Intelligence Research* 11 (1999) 1–94.
- [36] C. Boutilier, R. Dearden, M. Goldszmidt, Stochastic dynamic programming with factored representations, *Artificial intelligence* 121 (1-2) (2000) 49–107.
- [37] P. Spirtes, C. Glymour, R. Scheines, Causation, prediction, and search, MIT press, 2001.
- [38] N. R. Ke, O. Bilaniuk, A. Goyal, S. Bauer, H. Larochelle, B. Schölkopf, M. C. Mozer, C. Pal, Y. Bengio, Learning neural causal models from unknown interventions, *arXiv preprint arXiv:1910.01075* (2019).
- [39] Z. Wang, X. Xiao, Z. Xu, Y. Zhu, P. Stone, Causal dynamics learning for task-independent state abstraction, *arXiv preprint arXiv:2206.13452* (2022).
- [40] J. Runge, Causal network reconstruction from time series: From theoretical assumptions to practical estimation, *Chaos: An Interdisciplinary Journal of Nonlinear Science* 28 (7) (2018).
- [41] V. Mnih, K. Kavukcuoglu, D. Silver, A. A. Rusu, J. Veness, M. G. Bellemare, A. Graves, M. Riedmiller, A. K. Fidjeland, G. Ostrovski, et al., Human-level control through deep reinforcement learning, *nature* 518 (7540) (2015) 529–533.
- [42] M. Andrychowicz, F. Wolski, A. Ray, J. Schneider, R. Fong, P. Welinder, B. McGrew, J. Tobin, O. Pieter Abbeel, W. Zaremba, Hindsight experience replay, *Advances in neural information processing systems* 30 (2017).
- [43] A. Levy, G. Konidaris, R. Platt, K. Saenko, Learning multi-level hierarchies with hindsight, *arXiv preprint arXiv:1712.00948* (2017).

- [44] P.-L. Bacon, J. Harb, D. Precup, The option-critic architecture, in: Proceedings of the AAAI conference on artificial intelligence, Vol. 31, 2017.
- [45] W. Kim, J. Kim, Y. Sung, Lesson: learning to integrate exploration strategies for reinforcement learning via an option framework, arXiv preprint arXiv:2310.03342 (2023).